



Expression, purification, and spectral tuning of RhoGC, a retinylidene/guanylyl cyclase fusion protein and optogenetics tool from the aquatic fungus *Blastocladiella emersonii*

Received for publication, April 3, 2017, and in revised form, May 3, 2017. Published, Papers in Press, May 4, 2017, DOI 10.1074/jbc.M117.789636

Melissa M. Trieu^{†1}, Erin L. Devine^{†1}, Lindsey B. Lamarche[‡], Aaron E. Ammerman[‡], Jordan A. Greco[§], Robert R. Birge[§],
 Douglas L. Theobald^{†2}, and Daniel D. Oprian^{†3}

From the [†]Department of Biochemistry, Brandeis University, Waltham, Massachusetts 02454 and the [§]Departments of Chemistry and Molecular and Cell Biology, University of Connecticut, Storrs, Connecticut 06269

Edited by Henrik G. Dohlman

RhoGC is a rhodopsin (Rho)-guanylyl cyclase (GC) gene fusion molecule that is central to zoospore phototaxis in the aquatic fungus *Blastocladiella emersonii*. It has generated considerable excitement because of its demonstrated potential as a tool for optogenetic manipulation of cell-signaling pathways involving cyclic nucleotides. However, a reliable method for expressing and purifying RhoGC is currently lacking. We present here an expression and purification system for isolation of the full-length RhoGC protein expressed in HEK293 cells in detergent solution. The protein exhibits robust light-dependent guanylyl cyclase activity, whereas a truncated form lacking the 17- to 20-kDa N-terminal domain is completely inactive under identical conditions. Moreover, we designed several RhoGC mutants to increase the utility of the protein for optogenetic studies. The first class we generated has altered absorption spectra designed for selective activation by different wavelengths of light. Two mutants were created with blue-shifted (E254D, $\lambda_{\max} = 390$ nm; D380N, $\lambda_{\max} = 506$ nm) and one with red-shifted (D380E, $\lambda_{\max} = 533$ nm) absorption maxima relative to the wild-type protein ($\lambda_{\max} = 527$ nm). We also engineered a double mutant, E497K/C566D, that changes the enzyme to a specific, light-stimulated adenylyl cyclase that catalyzes the formation of cAMP from ATP. We anticipate that this expression/purification system and these RhoGC mutants will facilitate mechanistic and structural exploration of this important enzyme.

Retinylidene proteins comprise a family of integral membrane proteins composed of an apoprotein, opsin, covalently

This work was supported by National Institutes of Health Grants T32GM007596 (to E. L. D.), GM34548 (to R. R. B.), GM094468 and GM096053 (to D. L. T.), and EY007965 (to D. D. O.). The authors declare that they have no conflicts of interest with the contents of this article. The content is solely the responsibility of the authors and does not necessarily represent the official views of the National Institutes of Health.

¹ Both authors contributed equally to this work.

² To whom correspondence may be addressed: Dept. of Biochemistry, Brandeis University, 415 South St., Waltham, MA 02454. Tel.: 781-736-2303; E-mail: dtheobald@brandeis.edu.

³ To whom correspondence may be addressed: Dept. of Biochemistry, Brandeis University, 415 South St., Waltham, MA 02454. Tel.: 781-736-2322; E-mail: oprian@brandeis.edu.

bound to a retinal chromophore (1, 2). Amino acid sequence analysis divides the family into two groups known as type I and type II rhodopsins. Both groups share a G protein-coupled receptor fold, consisting of seven transmembrane α -helical segments that form a bundle in the membrane, with an extracellular N terminus and intracellular C terminus. The two groups also share an active-site Lys residue in the middle of the seventh transmembrane helix that is the site of covalent attachment to the chromophore, forming a Schiff base with the aldehyde moiety of the retinal.

Type II rhodopsins function primarily as photosensitive receptors in metazoan eyes and certain other non-ocular tissues. Rhodopsin, the photoreceptor of vertebrate rod cells, is a prototypic member of the G protein-coupled receptor family of membrane receptors (1, 2). The active site Lys-296 in rhodopsin covalently binds the 11-*cis* isomer of retinal to form a pigment with a visible absorption maximum at 500 nm. Upon exposure to light, the chromophore isomerizes to the all-*trans* form, and the absorption maximum shifts to 380 nm, indicative of the completion of the photoactivation sequence and the formation of the active metarhodopsin II form of the protein (3). Metarhodopsin II activates the G protein transducin, which then activates a cGMP phosphodiesterase. The resulting drop in cGMP levels in the cell closes cyclic nucleotide-gated channels in the membrane, and the rod cell hyperpolarizes to initiate an electrical signal in the retina (4). Vertebrate rhodopsin does not photocycle. The all-*trans* form of the chromophore must dissociate from the protein, and a new 11-*cis* retinal must bind to regenerate the dark state of the receptor.

Type I rhodopsins are of microbial origin (1, 2). The best-known example of this class of protein is bacteriorhodopsin (bR),⁴ the light-driven proton pump found in the archaeon *Halobacterium salinarum*. Type I rhodopsins typically photocycle, alternating between all-*trans* and 13-*cis* forms of the retinal chromophore, and function as light-driven ion transporters, channels, and phototaxis receptors coupled to two-component signaling pathways. Recently, the list of type I func-

⁴ The abbreviations used are: bR, bacteriorhodopsin; GC, guanylyl cyclase; Rho, rhodopsin; FL, full-length; RP, reverse-phase; T, truncated; DM, *n*-decyl- β -D-maltopyranoside; DDM, dodecyl maltoside; Nd:YAG, neodymium-doped yttrium aluminium garnet.

Purification and characterization of RhoGC

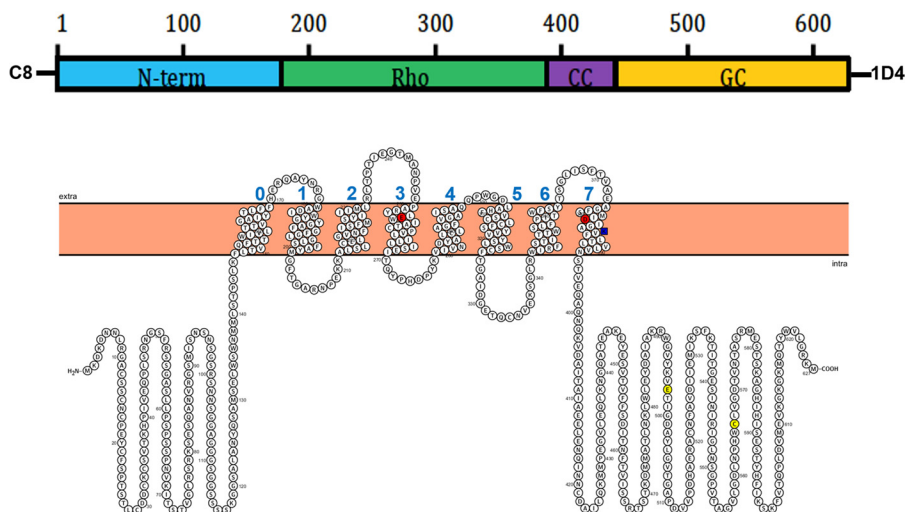


Figure 1. Predicted domain structure and transmembrane topography for RhoGC. The domains are as follows: *N-term*, N-terminal domain; *rho*, microbial type I rhodopsin domain; *CC*, coiled-coil domain; and *GC*, guanylyl cyclase domain. Transmembrane helices were predicted and drawn by Protter (wlab.ethz.ch/protter/start (25); please note that the JBC is not responsible for the long-term archiving and maintenance of this site or any other third party-hosted site). The amino acid residues are as follows: *red*, Glu-254 and Asp-380 counterions targeted for mutagenesis in the spectral tuning experiments; *blue*, Lys-384, presumed site of covalent attachment to the chromophore; *yellow*, Glu-497 and Cys-566, residues controlling the specificity for the GTP substrate.

tions has been expanded by the identification of a very unusual protein from the aquatic fungus *Blastocladiella emersonii* (5).

Zoospores of *B. emersonii* are phototactic, and the signaling pathway has been known for some time to involve cGMP. In 2014, Avelar *et al.* (5) identified a novel gene fusion (BeGC1) in which a type I (microbial) rhodopsin domain is fused to a C-terminal guanylyl cyclase (GC) catalytic domain (Fig. 1). The protein, hereafter referred to as RhoGC, localizes to the zoospore eyespot, and photobleaching of the rhodopsin domain or inhibition of the cyclase disrupts cGMP accumulation and inhibits zoospore phototaxis (5). Interestingly, the phototactic signaling pathway in *B. emersonii* shares similarities with the cyclic nucleotide pathway of vertebrate vision despite the fact that the rhodopsin domain of RhoGC is distantly related to the type II rhodopsins (5). The 2014 report by Avelar *et al.* (5) was followed quickly by two publications demonstrating the exciting potential of RhoGC to expand the tools available for optogenetic studies, particularly for controlling cyclic nucleotide signaling pathways (6, 7).

We present here an expression and purification system for the isolation of full-length (FL) RhoGC in detergent solution. The purified protein displays robust light-dependent guanylyl cyclase activity and a rapid photocycle with transient formation of intermediates with absorption maxima at 460 and 380 nm. We show that a truncated version of the protein missing the N-terminal domain is completely inactive. Finally, we present two groups of mutants designed to expand the utility of the protein in optogenetic studies: a group of spectral tuning mutants that hypso- and bathochromically shift the visible absorption maximum of the protein over a range of about 40 nm and a substrate specificity mutant that changes the protein from a guanylyl cyclase into an adenylyl cyclase.

Results

Expression and purification of FL RhoGC

Initial attempts at expression of RhoGC in bacteria and yeast were met with limited success. However, the protein did

express well in HEK293-GnT1⁻ cells despite the fact that the gene had been codon-optimized for *Escherichia coli*. The protein was purified from post-nuclear supernatant fractions of detergent-solubilized HEK293 cell extracts by immunoaffinity chromatography, making use of two epitope tags: C8 (PRGP-DRPEGIEE) (8) at the N terminus and 1D4 (TETSQVAPA) (9, 10) at the C terminus (see “Experimental Procedures”). Purification of the protein on the C8 column was followed by SDS-PAGE and Western blotting analysis (Fig. 2).

The purified RhoGC protein contains a major component that migrates on gels with an electrophoretic mobility corresponding to a molecular mass of about 70 kDa, consistent with that expected for the FL protein. At least some of the purified protein was FL, as demonstrated by the fact that the C8-purified protein reacts with the 1D4 antibody on Western blots (Fig. 2). The C8-purified protein contains variable amounts of an unidentified impurity that migrates with a mobility corresponding to a molecular mass of about 75 kDa. There is also a much smaller contaminant with an apparent molecular mass of 12–17 kDa (depending on the percentage of polyacrylamide in the gel) that is clearly an N-terminal proteolytic fragment of RhoGC because it reacts with the C8 antibody (Fig. 3C, lanes 1 and 2).

RhoGC is indeed susceptible to proteolytic degradation, as is apparent from the 50-kDa band in the 1D4-purified protein fraction on Coomassie-stained SDS gels (Fig. 3B, lane 1D4; visible also in the Western blot in Fig. 3D, lane 3). This 50-kDa fragment is henceforth referred to as T because it is a truncated form of the protein, missing the 20-kDa N-terminal domain. The purified preparation also contains a minor contaminant, visible on Western blots with the 1D4 antibody (Fig. 3D, lane 3), but not on the Coomassie-stained gel, which migrates with a mobility of about 30 kDa. The size of this peptide fragment is consistent with the molecular weight expected for the isolated guanylyl cyclase domain of the protein.

To ensure purification of the FL protein, we employed a sequential two-column immunoaffinity purification scheme

using both the N-terminal C8 and C-terminal 1D4 epitopes. Beginning with either the C8 or 1D4 columns, the sequential protocol results in highly purified FL protein, as shown in Fig. 3, *A*, lane 1D4, and *B*, lane C8, free of proteolytic contaminants.

In a typical protein preparation, we begin with 80 15-cm plates of transfected HEK293 cells containing an estimated 150 μg of RhoGC per plate (this is roughly double the molar expression level we see for bovine rhodopsin) for a total of 12 mg of RhoGC in the post-nuclear supernatant fraction from the detergent-solubilized cells. The yield of protein from the first 1D4 column is about 6.3 mg of rhoGC (based on absorbance at

530 nm), which includes both the full-length protein as well as the truncated form missing the 20-kDa N-terminal domain. This is fairly typical in that the yield from either the 1D4 or C8 column is generally about 50%, with most of the lost material remaining bound to the column in a state recalcitrant to elution with the synthetic peptides. Application of the 1D4-purified sample to a C8 column provides roughly 2.2 mg of truncated RhoGC, T, in the non-bound fraction and 1 mg of full-length RhoGC in the C8-peptide eluted fraction, again with a total yield from the antibody column of about 50% of the material applied.

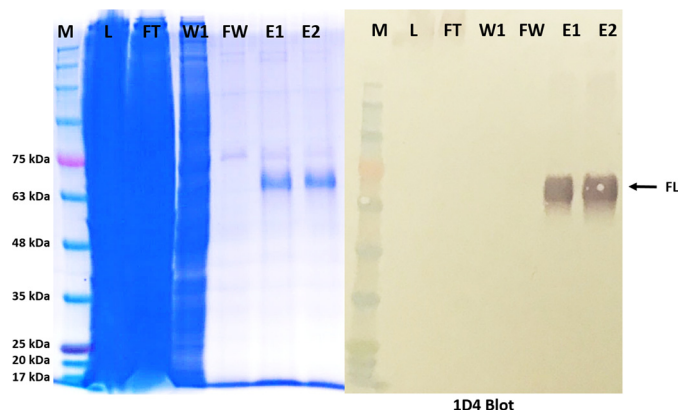


Figure 2. SDS-PAGE and Western blotting analysis of fractions obtained during immunoaffinity purification of RhoGC from transfected HEK293-GnT1⁻ cells. Shown are fractions from the purification of RhoGC with the C8 antibody. *A*, Coomassie-stained gel. *B*, Western blot of the same fractions as in *A* using the 1D4 antibody. *M*, molecular mass markers; *L*, load (post-nuclear supernatant fraction); *FT*, flow-through (non-bound fraction); *W1*, first wash; *FW*, final wash before elution; *E1*, first elution with C8 peptide; *E2*, second elution with the C8 peptide. *FL* indicates the position of FL RhoGC on the gel.

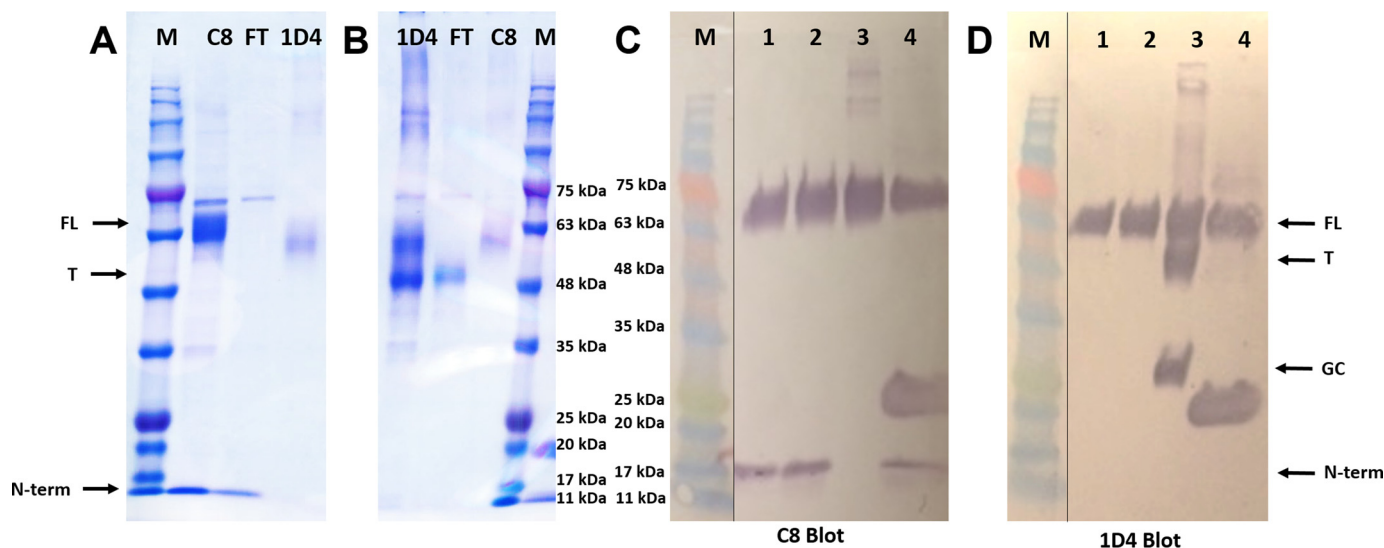


Figure 3. Purification of full-length (FL) and truncated (T) forms of RhoGC by tandem immunoaffinity chromatography on C8- and 1D4-antibody columns. *A*, Coomassie-stained gel of fractions from tandem immunoaffinity column purification using the C8 antibody first followed by the 1D4 antibody column. *B*, Coomassie-stained gel of fractions from tandem immunoaffinity column purification using the 1D4 antibody first followed by the C8 antibody column. *C*, Western blot of fractions using the C8 antibody as probe. *D*, Western blot of fractions using the 1D4 antibody as probe. Identifiers common to all panels: *M*, molecular mass markers; *FL*, full-length RhoGC; *T*, truncated RhoGC missing the N-terminal domain; *GC*, guanylyl cyclase domain; and *N-term*, the N-terminal domain. Purification presented in *panel A*: C8, eluent from the C8 column; *FT*, flow through, or non-bound fraction, from the C8 eluent applied to the 1D4 column; *1D4*, eluent from the 1D4 column. Purification presented in *panel B*: *1D4*, eluent from the 1D4 column; *FT*, flow through, or non-bound fraction, from the 1D4 eluent applied to the C8 column; *C8*, eluent from the C8 column. Fractions in *panels C* and *D* are from single-step purification using the C8 and 1D4 antibody columns: *lane 1*, eluent 1 from C8 column; *lane 2*, eluent 2 from C8 column; *lane 3*, eluent from 1D4 column; *lane 4*, SDS elution from the C8 column (intense band running with a mobility of about 25 kDa is the light chain of the C8 antibody). Molecular mass marker lanes were spliced as indicated by the dividing line. Note that the gels in *panels A* and *B* are 10% polyacrylamide while those in *panels C* and *D* are 12% polyacrylamide, which accounts for slight variation in the observed electrophoretic mobilities, particularly with respect to the N-terminal fragment.

Absorption spectrum

Purified RhoGC displays a visible absorption maximum at 527 nm (Fig. 4), with an extinction coefficient $\epsilon_{527} = 44,010 \text{ M}^{-1}\text{cm}^{-1}$, resulting from the retinal chromophore. Interestingly, the N-terminally truncated form of the protein, T, purified as a byproduct of the sequential scheme starting with the 1D4 column (Fig. 3*B*, lane *FT*), displays an identical absorption maximum at 527 nm.

Light-dependent guanylyl cyclase activity

As shown in Fig. 5, membrane preparations from HEK293-GnT1⁻ cells expressing RhoGC displayed robust light-dependent guanylyl cyclase activity, determined through analysis of reaction products by RP-HPLC. The enzyme was off in the dark, turned on quickly with light, and turned off quickly again when the light was removed, demonstrating that RhoGC is a tightly regulated protein that does not produce cGMP in the absence of light. The amount of RhoGC in the membrane preparations was quantified by Western blotting analysis using the

Purification and characterization of RhoGC

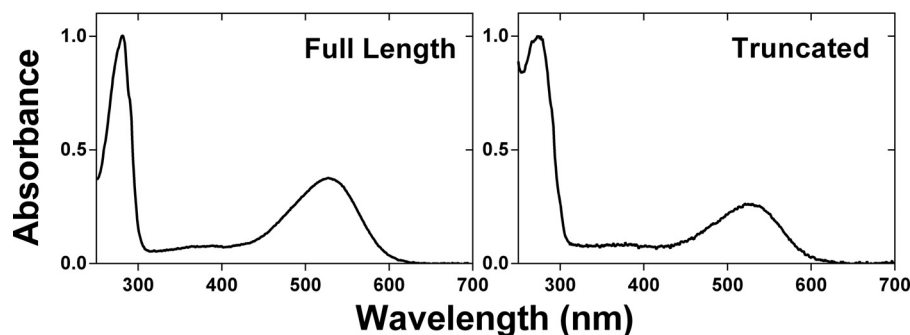


Figure 4. Absorption spectra for RhoGC expressed in and purified from transfected HEK293-GnT1⁻ cells. A, FL RhoGC purified by tandem immunoaffinity chromatography on C8 and 1D4 antibody columns. B, truncated RhoGC purified from the non-bound fraction of a 1D4 column after loading C8-purified RhoGC. The spectra have been normalized for absorbance at 280 nm.

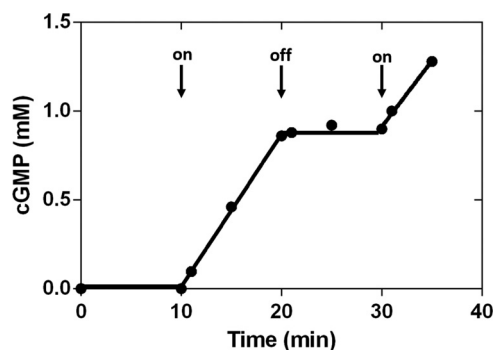


Figure 5. Light-dependent guanylyl cyclase activity of RhoGC in membranes isolated from transiently transfected HEK293-GnT1⁻ cells. Each reaction contained 0.85 μM RhoGC, as determined by Western blotting analysis of the membranes. The formation of cGMP from GTP (5 mM) was followed by HPLC. The reaction was allowed to proceed for 10 min in the dark, after which the reaction was exposed to light (first arrow) from a 300-W tungsten bulb filtered through a 475-nm cut-on filter. The reaction was returned to the dark at 20 min and exposed to light again at 30 min, as indicated by the second and third arrows, respectively.

1D4 antibody, which enabled a determination of $k_{\text{cat}} = 1.7 \text{ s}^{-1}$ for the enzyme under these assay conditions.

To avoid exposing the RP-HPLC column to detergent, an alternate assay was employed for purified RhoGC that used autoradiography to quantify GTP and cGMP after separation on TLC plates. This assay was conveniently performed under substrate depletion conditions to monitor the complete time course and to determine both K_m and k_{cat} from a single reaction using the integrated form of the Michaelis-Menten equation (Fig. 6A). The k_{cat} determined in this assay ($2.2 \pm 0.4 \text{ s}^{-1}$) agrees well with that determined for RhoGC in membranes, whereas the K_m for GTP ($0.9 \pm 0.3 \text{ mM}$) agrees well with Michaelis constants reported for related guanylyl cyclases (11). It is noteworthy that the enzyme retains its light-dependent activity in detergent solution; it is off in the dark, turns on quickly with light, and turns off quickly again when the light is removed (Fig. 7A).

The substrate depletion assay, although convenient, could be unsuitable for following the activity of RhoGC when the enzyme is subject to product inhibition by cGMP. As can be seen from a comparison of Fig. 6, A and B, the k_{cat} , K_m , and entire time course for the reaction are unaffected by the presence of 1 mM cGMP product in the reaction mixture (product inhibition was not explored with pyrophosphate because of its limited solubility in aqueous solution). Furthermore, we com-

pared the kinetics for the reaction determined from the substrate depletion assay with those determined for the enzyme under initial rate conditions. As can be seen in Fig. 7B, there is very good agreement between the two, suggesting that the two assays are interchangeable. Thus, RhoGC does not exhibit product inhibition.

The detergent-compatible assay also permitted the measurement of activity for the truncated form of the protein, T. As can be seen in Fig. 7C, T is completely inactive under the same conditions where the FL protein displays robust light-dependent guanylyl cyclase activity, suggesting that the N-terminal domain of RhoGC performs an important structural role in enabling communication of the rhodopsin and guanylyl cyclase domains of the protein.

Photointermediates

Time-resolved spectral changes were followed for both the FL and T forms of RhoGC after initiating the reactions with a 5-ns pulse from a 532-nm neodymium:YAG laser. Difference spectra for the reactions of both proteins recorded every 1 ms for the first 1.1 s of the reaction showed that there is a rapid decrease in absorbance at 527 nm with a concomitant increase at 380 nm in the first 20–30 ms, followed by a slower recovery phase over the next 200 ms (Fig. 8, A, B, D, and E). The intermediate with a 380-nm maximum is presumably the active species with an unprotonated Schiff base in the chromophore. The single-wavelength kinetic trace at 380 nm for formation and decay of the intermediate from the FL protein (Fig. 8C) was well fit by two exponentials with a time constant for formation of 12 ms and decay of 100 ms.

The reaction with the truncated form, T (Fig. 8F), is similar but with time constants representing slightly faster rates of formation and decay (8 and 74 ms, respectively). Although the single wavelength data at 380 nm were fit well by two exponentials, the reaction is clearly more complex than what is represented by this simple model. Difference spectra (light versus dark) for the FL protein show the presence of a prominent intermediate, with a maximum at about 460 nm formed early in the reaction sequence that is not accounted for with the simple two-exponential kinetic scheme. Although the single-wavelength reaction time course at 380 nm was similar for FL and T, the time-resolved difference spectra (Fig. 8, A and D) show significant differences in the reactions of the two proteins. We also note that the single wavelength data were fit to an equation with

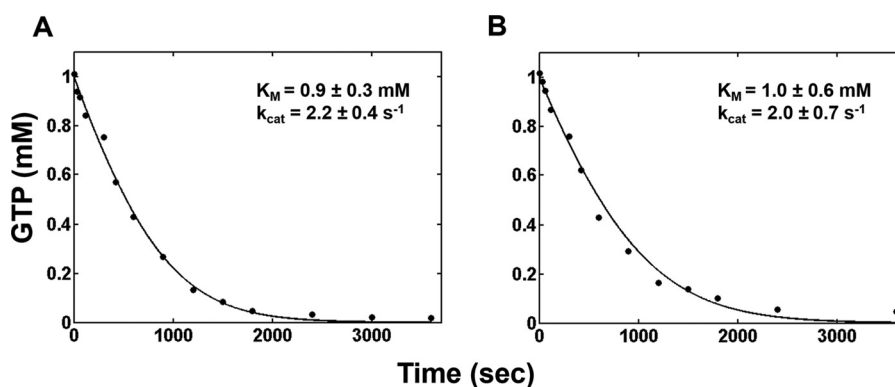


Figure 6. Substrate depletion assay for reaction of FL RhoGC with $[\alpha\text{-}^{32}\text{P}]\text{GTP}$ in detergent solution. *A*, the reaction consisted of $1\ \mu\text{M}$ RhoGC and $1\ \text{mM}$ $[\alpha\text{-}^{32}\text{P}]\text{GTP}$ ($0.02\ \text{Ci}/\text{mmol}$) in $50\ \text{mM}$ Tris buffer (pH 8.0) containing $50\ \text{mM}$ NaCl, $10\ \text{mM}$ MgCl_2 , $0.5\ \text{mM}$ EDTA, and 0.1% DM (w/v). *B*, the same as in *A*, except the reaction also contained $1\ \text{mM}$ cGMP product. The reaction was initiated by exposure to continuous illumination from a 300-W tungsten lamp filtered through a 475-nm cut-on filter. The data (discrete points) were fit (solid line) to the integrated form of the Michaelis-Menten equation using the COPASI biochemical system simulator software (<http://www.copasi.org> (26, 27); please note that the JBC is not responsible for the long-term archiving and maintenance of this site or any other third party-hosted site), from which the K_m and k_{cat} for the enzyme were determined.

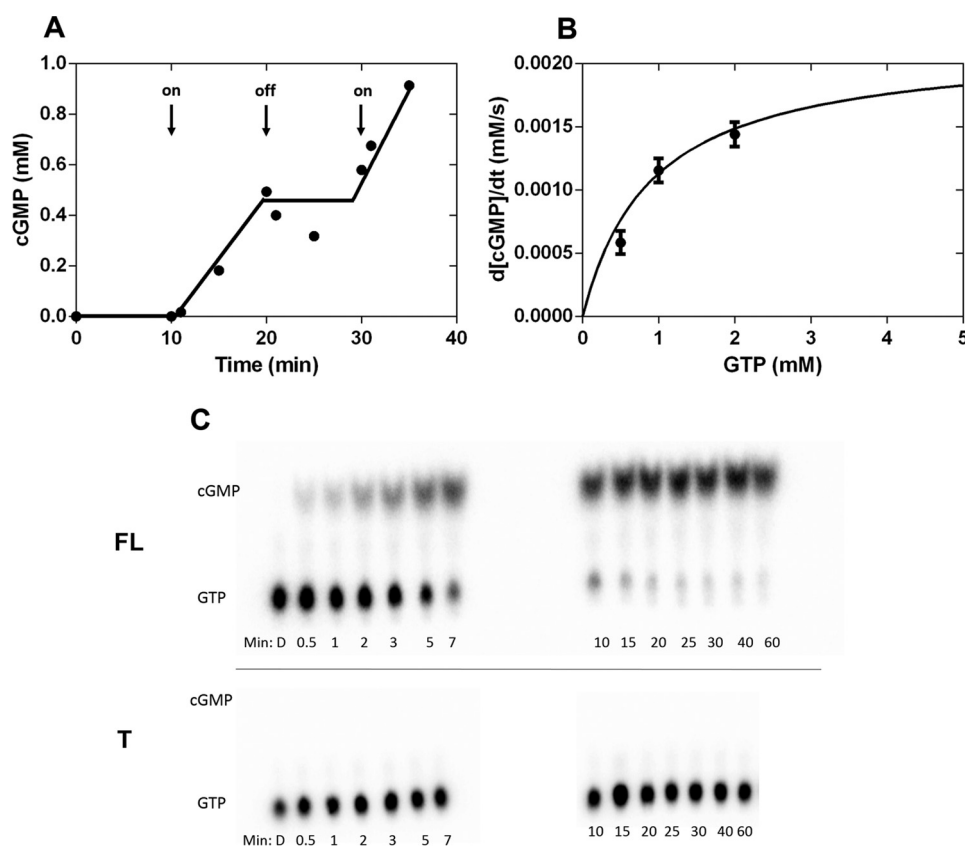


Figure 7. Characterization of the radioactivity-based assay for guanylyl cyclase activity in detergent solution. *A*, dependence of enzyme activity on light. *On* and *off* arrows indicate the times at which the 300-W tungsten bulb was turned on and off, respectively. *B*, comparison of the Michaelis-Menten curve (solid line), calculated using k_{cat} and K_m from the substrate depletion assay (Fig. 6), with initial rate data (data points) from reactions under the same conditions but starting with different initial concentrations of the GTP substrate. *C*, comparison of raw PhosphorImager images of PEI-cellulose plates for assays of the FL and T forms of RhoGC.

a third exponential term with a long time constant ($\tau \sim 8\ \text{s}$) to account for the fact that, after each flash, a certain fraction of the protein remained in a 380-nm state, never returning to the dark state with maximum at $527\ \text{nm}$.

Membrane orientation and topology of RhoGC

Although microbial rhodopsins typically have seven transmembrane α helices, hydrophathy analysis with Protter software

predicted an additional helix for RhoGC, suggesting that the N and C termini of the protein were both located on the cytoplasmic side of the membrane (Fig. 1). To test this proposed topology and orientation, we transfected CHO cells with the gene for RhoGC in which the N and C termini were tagged with the C8 and 1D4 epitopes, respectively. As can be seen in Fig. 9, both the C8 and 1D4 antibodies reacted with transfected CHO cells only after the cell membranes were first permeabilized with Triton

Purification and characterization of RhoGC

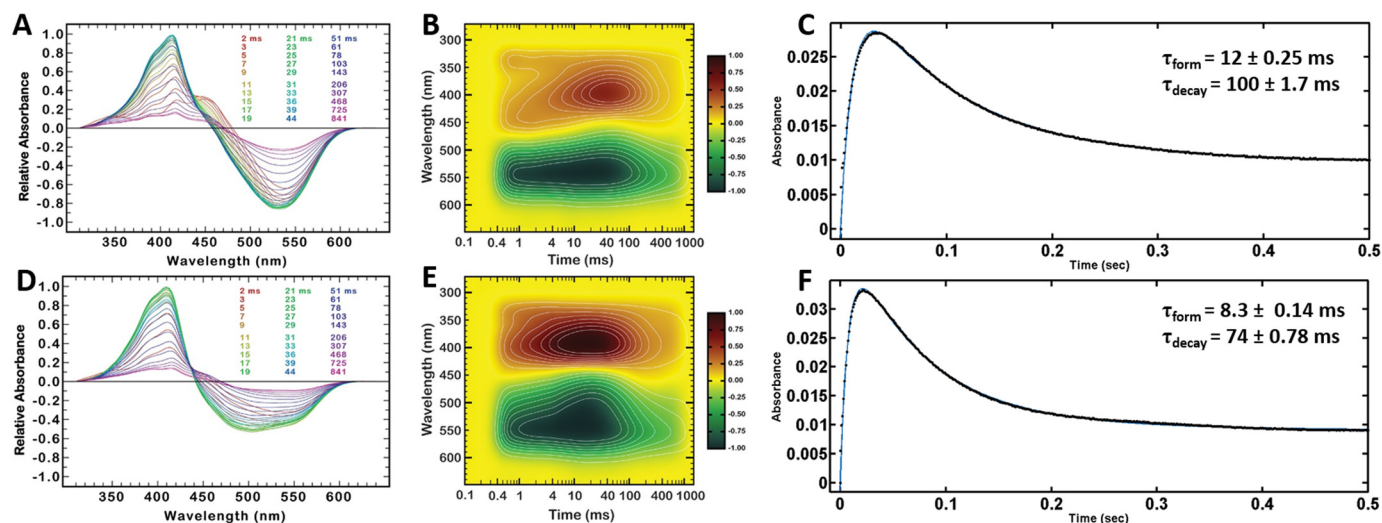


Figure 8. A–F, time-resolved spectral changes for FL (A–C) and truncated (D–F) forms of RhoGC. A and D, time-resolved difference spectra recorded every millisecond for the first 1.1 s of reaction following a 5-ns pulse from a 532-nm laser (25 mJ/pulse). Time is encoded by color, as indicated in the inset. Selected spectra were omitted for clarity. B and E, heat maps for time-dependent evolution of spectral changes. Relative absorbance is color-coded as illustrated in the side bar. C and F, single-wavelength time course for the reaction monitored at 380 nm. Experimental data are shown as discrete points, whereas the fit using Equation 1 (see “Experimental Procedures”) with the indicated time constants is shown as a solid line. All data were collected at 25 °C in DDM solution.

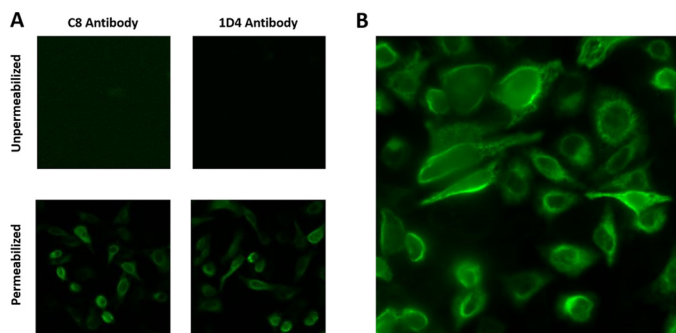


Figure 9. Determination of RhoGC transmembrane topology and orientation. A, immobilized CHO K-1 cells were transfected with the dual (C8 and 1D4) epitope-tagged RhoGC on glass coverslips and incubated with the antibodies under permeabilized or unpermeabilized conditions for immunofluorescent staining as indicated and as described under “Experimental Procedures.” Both C8 and 1D4 antibodies react with RhoGC, but only after the cells are first permeabilized with detergent, indicating that the N and C termini are located intracellularly. B, a higher-magnification view of the 1D4-stained cells, clearly showing a diffuse staining pattern typical of proteins localized to the plasma membrane.

X-100, demonstrating clearly that the N and C termini of the protein are both located on the cytoplasmic surface of the cell membrane, consistent with the prediction of eight transmembrane segments. It is important for the interpretation of these results that RhoGC displays the diffuse staining pattern typical of proteins located in the plasma membrane (Fig. 9B) rather than a punctate pattern, suggesting that the protein was retained within membranes of the cell interior.

RhoGC specificity and spectral tuning mutants

Mutagenesis studies designed to expand the use of RhoGC in optogenetic applications targeted two properties of the protein: the absorption spectrum of the retinal chromophore and the substrate specificity controlling identity of the cyclic nucleotide product. Two amino acid residues, Glu-254 and Asp-380, in RhoGC were targeted for mutation in spectral tuning studies because the homologous residues, Asp-85 and Asp-212, are known to be important for the spectral properties of bR (12, 13).

As can be seen in Fig. 10, mutation of these residues results in relatively dramatic shifts in the spectral properties of the chromophore, which, in the WT protein, is centered at 527 nm. E254D displays a blue-shifted λ_{\max} = 490 nm and a prominent shoulder at about 460 nm. The D380N mutant is also blue-shifted, with λ_{\max} = 506 nm, whereas changing Asp-380 to Glu in the D380E mutant results in a red-shifted λ_{\max} = 533 nm. These three mutant proteins have expanded the range of λ_{\max} in the chromophore to cover a little more than 40 nm. Significantly, all of the mutants retain light-dependent guanylyl cyclase activity, as measured in cell membranes isolated from transfected HEK293 cells. No reaction was observed in the absence of illumination, and the activities relative to the WT (= 1.0) were as follows: D380E, 0.43; E254D, 0.17; D380N, 0.093. The range of activities relative to the WT protein reflect a combination of intrinsic activity, expression level, and position of absorption band relative to the 435-nm cut-on filter used for illumination of the reaction mixtures. No attempt was made to sort out these various factors, as the crucial observation was that all mutants were active, and the activity was completely dependent upon exposure to light.

Two additional amino acids, Glu-497 and Cys-566 in the guanylyl cyclase domain, were targeted for mutation because these residues have been shown to control substrate specificity in other guanylyl and adenylyl cyclases (14, 15). As seen in Fig. 11A, the E497K/C566D double mutant converts RhoGC into a light-activated adenylyl cyclase, shifting the substrate specificity from GTP to ATP. The mutant has a 10-fold lower k_{cat} than the WT and also displays dark activity not observed in the WT enzyme. However, the mutant enzyme is completely specific for the ATP substrate. Both single mutants, E497K and C566D, are completely inactive with either substrate, GTP or ATP, as one might expect. It is also noteworthy that the mutations at positions 497 and 566 do not affect the spectral properties of the retinal chromophore (Fig. 11B), suggesting that the adenylyl cyclase mutations can be combined with the spectral tuning

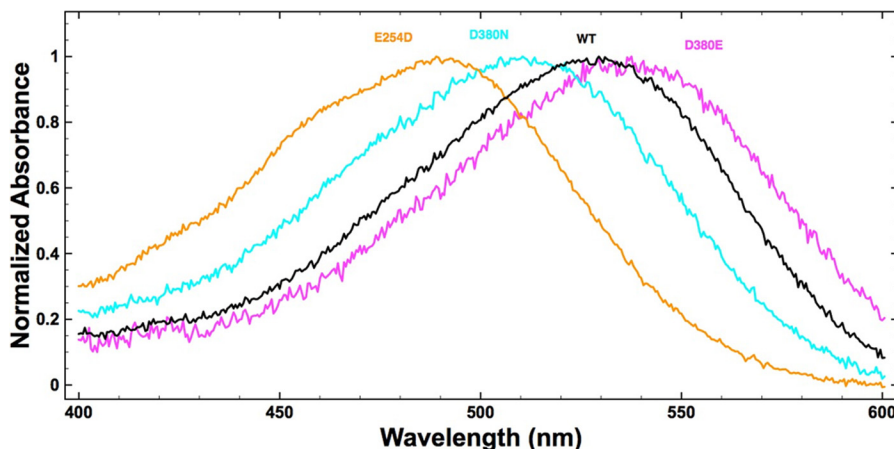


Figure 10. Normalized absorption spectra for spectral tuning mutants. In order of increasing λ_{max} , shown are E254D (orange), D380N (cyan), WT (black), and D380E (magenta). Absorption maxima were determined for each dataset from the derivative of a second-order polynomial fit to the data over a limited wavelength range surrounding λ_{max} in the visible region of the spectrum: E254D (510–480 nm), $\lambda_{\text{max}} = 490.1 \pm 0.2$; D380N (540–480 nm), $\lambda_{\text{max}} = 509.3 \pm 0.1$; WT (550–510 nm), $\lambda_{\text{max}} = 527.4 \pm 0.1$; and D380E (555–520 nm), $\lambda_{\text{max}} = 536.3 \pm 0.3$. The precision with which the λ_{max} values were determined reflects not only noise in the original spectrum but also the wavelength range (*i.e.* number of data points) used for the polynomial fit.

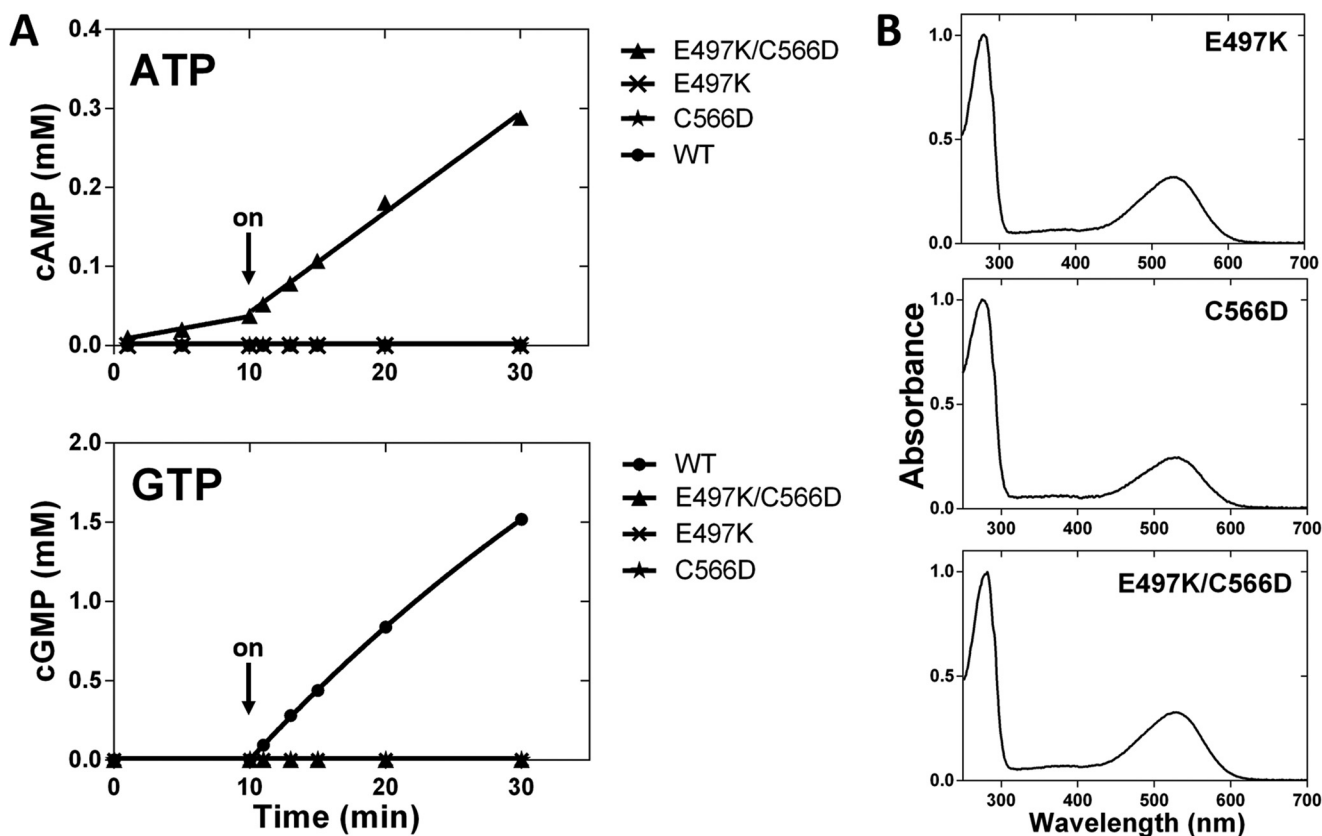


Figure 11. Adenylyl cyclase mutants. *A*, determination of substrate specificity for WT RhoGC and the E497K, C566D, and E497K/C566D mutants. Reactions contained $0.85 \mu\text{M}$ RhoGC (WT or mutant) in membranes from transfected HEK293 cells and either GTP or ATP at 5 mM initial concentration, as indicated. Time points were collected over the first 10 min in the dark and then (arrow) under continuous exposure to light from a 300-W tungsten bulb with a 475-nm cut-on filter over the next 20 min. Cyclic nucleotides (cGMP and cAMP) were followed by HPLC as described under “Experimental Procedures.” The E497K/C566D double mutant displays some constitutive activity in the dark but has clearly had its substrate specificity changed to that of an adenylyl cyclase and exhibits 4-fold stimulation of activity by light. *B*, UV-visible absorption spectra for E497K, C566D, and the double mutant E497K/C566D. Spectra have been normalized to optical density = 1.0 at 280 nm.

mutants without adverse effects on the enzyme activity or spectral properties of the chromophore.

Discussion

The main focus of this study was to develop an expression and purification system for the FL rhodopsin/guanylyl cyclase

fusion protein, RhoGC, from *B. emersonii* (5). The gene for the protein was expressed to high levels in HEK293-GnT1⁻ cells in culture, and the protein was purified to near homogeneity, free of proteolytic contaminants, by a tandem immunoaffinity chromatography protocol that used two different epitope tags: C8 (8) at the N terminus and 1D4 (9, 10) at the C terminus of the

Purification and characterization of RhoGC

protein. Purification of the FL protein is an important first step in developing an in-depth mechanistic investigation of the protein, as it allows spectroscopic tools to be applied under the same conditions as assays to monitor enzymatic activity. It is also a prerequisite for the determination of structure.

The FL purified protein displays a visible absorption maximum at 527 nm. An identical spectrum was observed for the truncated protein lacking the N-terminal domain, as reported here, and a truncated form containing only the membrane-embedded rhodopsin domain expressed in and purified from *Pichia pastoris* (7). These data agree well with the wavelength dependence for phototaxis of *B. emersonii* zoospores originally reported by Avelar *et al.* (5) and with action spectra for membranes isolated from *Xenopus* oocytes expressing RhoGC (6). In addition, we have shown that the FL protein displays robust light-dependent guanylyl cyclase activity in DM solution, with a similar k_{cat} (about 2 s^{-1}) as that of the enzyme in isolated membranes from HEK293 cells (shown here) and *P. pastoris* (7) and a K_m (about 1 mM) similar to that reported for other guanylyl cyclases (11).

The RhoGC photocycle shows rapid formation and decay of an intermediate with a maximum in the difference spectrum at 380 nm. The intermediate forms with a time constant of 12 ms and decays with a time constant of 100 ms and is presumably the active form of the enzyme. The T form of RhoGC displayed similar single wavelength kinetics at 380 nm and exhibited time-dependent difference spectra reminiscent of those described for the truncated form isolated from *P. pastoris* (7). However, T has significantly different time-dependent spectra compared with the FL protein. In particular, the reaction with the T form lacks the 460-nm intermediate seen with the FL protein. This result is perhaps not surprising because the T form also lacks enzymatic activity. A more in-depth analysis of the photocycle is beyond the scope of this study but will be the focus of future efforts with this enzyme.

The gene construct with two epitope tags on RhoGC permitted an easy determination of transmembrane topology for the N and C termini of the protein in intact CHO K1 cells. Both the C8 and 1D4 antibodies reacted with the protein in the plasma membrane of transfected cells but only after the membranes were first permeabilized with Triton X-100. These data demonstrate that both the N and C termini of the protein reside on the cytoplasmic side of the plasma membrane, consistent with the prediction of eight transmembrane helices first proposed and experimentally documented by Gottschalk and co-workers (6) using bimolecular fluorescence complementation with split YFP constructs fused to the N and C termini of RhoGC ectopically expressed in *Xenopus* oocytes. The cytoplasmic location of the N terminus of RhoGC suggests that the N terminus may interact with the C-terminal guanylyl cyclase domain. If correct, this may help explain several observations: an N-terminal deletion of the first 90 amino acids results in a constitutively active guanylyl cyclase with little dependence on light (6), a larger N-terminal deletion of the first 138 amino acids results in a protein with little remaining cyclase activity (7), and our finding that the proteolytic fragment missing the N-terminal domain (T, isolated as a byproduct of purification of the FL protein) is completely inactive under conditions in which the

FL protein displays robust cyclase activity. These data are all the more interesting given the fact that the absorption spectrum of the truncated protein is identical to that of the FL RhoGC.

The amino acid residues Glu-254 and Asp-380, selected for spectral tuning sites in RhoGC, were chosen because these two positions serve as counterion residues to the protonated Schiff base of the retinal chromophore in bR and because mutation of these amino acids results in large changes to the visible absorption peak in the archaeobacterial protein (12, 13). The spectroscopic effect of the mutations in RhoGC were qualitatively similar to the corresponding substitutions in bR: Glu at position 254 (85 in bR) is shifted to the blue relative to Asp, Asn at position 380 (212 in bR) is shifted to the blue relative to Asp, and Glu is shifted to the red (12, 13). Although the red-shifted spectra are of interest for optogenetic studies because of the greater tissue penetration of red light in intact animals, the blue-shifted mutants are also of interest because they help expand the range of wavelengths that can be exploited to selectively activate various mutants of the WT protein.

Finally, the two amino acid residues that change the substrate specificity of RhoGC from GTP to ATP were chosen based on previous work with related guanylyl and adenylyl cyclases. The crystal structure of the catalytic domain of an adenylyl cyclase (VC₁IIC₂) in complex with G_{sα}-GTPγS and 2'd3'-AMP suggests that two amino acid residues, Lys-938 and Asp-1018, confer specificity for the ATP substrate (16). Independently, GTP and ATP were docked into a homology model of the catalytic domain of the guanylyl cyclase RetGC based on the crystal structure of a C2 domain homodimer of a type II adenylyl cyclase. This *in silico* work identified the corresponding residues, Glu-925 and Cys-995, as specifying substrate selectivity for GTP (17). Subsequent mutagenesis studies showed that making the Glu-to-Lys and Cys-to-Asp double mutant converted both the membrane-bound RetGC (15) as well as a soluble guanylyl cyclase (14) into ATP-specific adenylyl cyclases. The corresponding amino acids in RhoGC are Glu-497 and Cys-566. In agreement with the earlier studies, the mutations in the RhoGC double mutant, E497K/C566D, convert the enzyme from a guanylyl cyclase to an adenylyl cyclase. Although the change coincides with an increase in dark activity for the enzyme, the mutant protein should nevertheless be useful for expanding the optogenetic utility of RhoGC to controlling intracellular cyclic nucleotides in signaling systems utilizing cAMP. Future work will focus on decreasing the dark activity of the mutant enzyme. In conclusion, we hope that the spectral tuning and substrate selectivity mutants described here will be of use in optogenetic applications of RhoGC, and we anticipate that the expression/purification system will facilitate structural and mechanistic exploration of this interesting enzyme.

Experimental procedures

Materials

All-*trans* retinal was purchased from Sigma-Aldrich. *n*-Decyl-β-D-maltopyranoside (DM) was from Anatrace. Dodecyl maltoside (DDM) was from Calbiochem. Bovine growth serum and Dulbecco's PBS were from HyClone Laboratories. DMEM was purchased from Gibco. GTP was from Amersham Biosci-

ences. ATP was from Pharmacia. and [α - 32 P]GTP (3000 Ci/mmol) was from PerkinElmer Life Sciences. The oligonucleotides used for the addition of antibody tags and mutagenesis were purchased from Integrated DNA Technologies. The C8 (8) and 1D4 (9, 10) antibodies were from the National Cell Culture Center (Minneapolis, MN). The C8- and 1D4-Sepharose 4B immunoaffinity matrices used to purify the pigments were prepared as described previously (18, 19). C8 and 1D4 peptides, used to elute protein from the immunoaffinity matrices, were purchased from GenScript.

Expression and purification

The gene for RhoGC was from *BeGC1* (accession number KF309499) and had been codon-optimized for expression in *E. coli* (Genewiz Inc., South Plainfield, NJ). The gene was inserted between the EcoRI and NotI restriction sites of the mammalian expression vector pMT3 (20). Epitope tags were added at the N terminus (C8 epitope, placed between amino acids 1 and 2 of the native sequence) and C terminus (a GSGS linker followed by a T9A mutant of the 1D4 epitope was added after the last amino acid of the native sequence). Mutations were introduced by QuikChange II site-directed mutagenesis (Agilent).

The expression and purification of RhoGC and mutants were performed essentially as described previously for bovine rhodopsin (20). Proteins were expressed transiently in HEK293-GnT1⁻ cells by using calcium phosphate precipitation for transfection, and cells were harvested 72 h post-transfection. All-trans retinal (10 μ M) was added to the cell suspension in the dark, followed by an incubation period of 30 min at 4 °C. All procedures following the addition of retinal were performed in the dark under a dim red light. Cells were lysed in 2% DDM or DM detergent for 1 h at 4 °C. The lysate was centrifuged at 3500 rpm and 4 °C for 10 min to remove nuclei, and the post-nuclear supernatant fraction was applied to an immunoaffinity matrix (either anti-C8 or anti-1D4). The proteins were allowed to bind to the column for 2 h at 4 °C before the non-bound fraction was removed. The column was then washed at 4 °C with 0.1% (w/v) detergent (DM or DDM) in PBS. Purified protein was eluted at room temperature with 80 μ M peptide (C8 or 1D4).

Absorption spectroscopy

UV-visible absorption spectra were recorded with a Cary 50 UV-visible spectrometer at room temperature using a path length of 1.0 cm. The molar extinction coefficient for RhoGC ($\epsilon_{527} = 44,010 \text{ M}^{-1}\text{cm}^{-1}$) was determined by acid-trapping the chromophore ($\epsilon_{440} = 31,000 \text{ M}^{-1}\text{cm}^{-1}$) in the dark with HCl as described previously (21). Absorption maxima for WT RhoGC and the three spectral tuning mutants shown in Fig. 10 were determined from the derivative of a second-order polynomial fit to a part of the spectrum containing a limited range of wavelengths surrounding the maximum.

Preparation of HEK293 cell membranes

HEK293-GnT1⁻ cell membranes containing RhoGC were prepared as described previously for COS cell membranes containing rhodopsin (22). Briefly, cells were harvested 72 h after transfection and washed with PBS before being lysed hypoton-

ically in a solution containing 10 mM Tris buffer (pH 7.4) and 0.1 mg/ml phenylmethylsulfonyl fluoride. The cells were further disrupted by passing the suspension through a 25-gauge needle four times. The homogenate was layered onto a cushion of 37% (w/v) sucrose in 10 mM Tris buffer (pH 7.4) containing 150 mM NaCl, 1 mM MgCl₂, 1 mM CaCl₂, and 0.1 mM EDTA and centrifuged in a Beckman SW 28.1 rotor for 20 min at 15,000 rpm. Membranes were collected from the interface, diluted 10-fold in 10 mM Tris buffer (pH 7.4), and pelleted by centrifugation in a Beckman 50.2 Ti rotor for 45 min at 33,000 rpm. The pellet was resuspended in 1 ml of 10 mM Tris buffer (pH 7.4), 150 mM NaCl, 1 mM MgCl₂, 1 mM CaCl₂, and 0.1 mM EDTA, frozen on dry ice, and stored until use at -80 °C. The concentration of RhoGC was quantified by Western blots using the 1D4 antibody.

Assay for guanylyl cyclase activity: HPLC

We used two different assays for guanylyl cyclase activity: a reverse-phase HPLC (RP-HPLC) assay (described here), in which RhoGC was provided in HEK293 cell membranes, and a radioactivity-based assay, in which purified RhoGC was provided in detergent solution (see below). Membranes for the HPLC-based assay were prepared from HEK293 cells containing RhoGC, as described above, and then incubated with 10 μ M all-trans retinal at room temperature for 30 min before being used in the assay. The 1-ml (total volume) reaction, consisting of 0.85 μ M RhoGC in 50 mM Tris-based buffer (pH 8.0), 50 mM NaCl, 10 mM MgCl₂, and 0.5 mM EDTA, was initiated by addition of 5 mM GTP. Time points (100 μ l each) were first taken for the reaction in the dark, followed by time points after the reaction mixture was exposed to light from a 300-W tungsten bulb with a 475-nm cut-on filter (435-nm cut-on filter for the spectral tuning mutants). The reaction for each time point was quenched with 100 μ l of 0.2 M EDTA, the sample was filtered through a 10-kDa cut-off membrane (Amicon), and the filtered solution (5 μ l) was then injected onto a 250 \times 2.1 mm ACE 5 C18-AR reverse-phase 5- μ m column of an Agilent 1260 Infinity HPLC system with a G136D 1260 multiwavelength detector. The column was developed with a solvent of 100 mM potassium phosphate buffer (pH 6.2) at a flow rate of 0.4 ml/min. Nucleotides were monitored at 254 nm and analyzed with OpenLab CDS ChemStation software for integration of the peaks using known standards of GTP and cGMP.

Assays for adenylyl cyclase activity were performed identically, except that the reaction was initiated by addition of 5 mM ATP instead of GTP, and the HPLC column running buffer was 100 mM potassium phosphate (pH 6.2) containing 10% (v/v) methanol. The concentration of stock solutions was determined spectrophotometrically using the following extinction coefficients ($\text{M}^{-1}\text{cm}^{-1}$): GTP, 13,700 at 252 nm; cGMP, 12,320 at 260 nm; ATP, 15,400 at 259 nm; and cAMP, 15,000 at 260 nm.

Assay for guanylyl cyclase activity: Radioactivity

Radioactive [α - 32 P]GTP was used to follow the progress of the reaction when guanylyl cyclase assays were performed with purified RhoGC in detergent solution. The reaction mixture consisted of 1 μ M RhoGC and 1 mM [α - 32 P]GTP (0.02

Purification and characterization of RhoGC

Ci/mmol) in 50 mM Tris buffer (pH 8.0) containing 50 mM NaCl, 10 mM MgCl₂, and 0.5 mM EDTA. Samples were kept in the dark for 10 min and then illuminated with a 300-W tungsten bulb through a 475-nm cut-on filter. Aliquots (2 μl) were removed at various times and quenched by addition of 8 μl of 0.2 M EDTA. Samples were then spotted on a PEI-cellulose TLC plate that was developed with 1 M LiCl to separate cGMP from GTP. The amount of radioactivity in each spot was quantified with a GE PhosphorImager screen and Typhoon 9410 imaging system using ImageQuant TL 7.0 software and a standard curve of known samples. The reaction was either run to completion until all of the substrate was converted to product or under initial rate conditions following the linear formation of product with time for the first 15 s of reaction at different initial concentrations of substrate.

Transmembrane topology

The transmembrane topology of RhoGC was interrogated using transfected CHO cells (23). CHO-K1 cells (RRID, CVCL_0214) were purchased from the ATCC (Manassas, VA), identity-authenticated by cytochrome oxidase one analysis, demonstrated to be mycoplasma-free by Hoechst DNA stain and agar by culture, and maintained in F12K medium supplemented with 10% FBS (ATCC). Cells were plated on L-lysine-coated coverslips, grown to a confluency of 80%, and transfected with RhoGC in the pMT3 expression vector (along with pRSV-TAg containing the large T antigen) using Lipofectamine 2000 (Thermo Fisher) according to the protocol of the manufacturer. After 24 h, the cells were fixed with 4% (v/v) paraformaldehyde in PBS for 15 min at room temperature, washed twice with ice-cold PBS, and then either treated directly with ice-cold 10% (w/v) BSA in PBS for 30 min or first permeabilized by incubation with 0.25% (v/v) Triton X-100 in PBS for 10 min at room temperature and then treated with BSA as indicated above. The cells were washed three times with cold PBS, treated with BSA again, and then incubated with 2 μg/ml primary antibody (either C8 or 1D4) in PBS containing 10% (w/v) BSA at room temperature for 1 h. The cells were then washed three times with cold PBS before adding an Alexa Fluor 488 goat anti-mouse IgG secondary antibody (Life Technologies) at 2 μg/ml in PBS and incubation 1 h at room temperature in the dark. The coverslips were washed three times with ice-cold PBS and prepared for imaging by applying to a glass slide with ProLong Diamond Antifade Mountant (Life Technologies).

The CHO-K1 cells were imaged using an automated Olympus IX81 epifluorescence microscope (Olympus, Waltham, MA). Alexa Fluor 488 was excited using a mercury vapor short-arc lamp (Excelitas Tech) via a 473/31-nm bandpass filter (Semrock, Rochester, NY), and the emission was collected through a 520/25-nm bandpass filter (Semrock). Images were captured using an EM charge-coupled device (CCD) camera (Hamamatsu, Japan) controlled by Metamorph (Molecular Devices, Sunnyvale, CA) and analyzed with ImageJ software (National Institutes of Health, Bethesda, MD).

Time-resolved absorption spectroscopy

Each RhoGC sample was concentrated to 23 μM for an optical density of 1.0 at the absorption maximum ($\lambda_{\text{max}} = 527$ nm)

in PBS containing 0.1% DDM and transferred to a 1-cm path length, 1.5-ml methacrylate cuvette (Plastibrand cuvettes, Fisher Scientific, Inc.). The actinic pump pulse for each time-resolved measurement was supplied by 532-nm, 5-ns pulse width emission from a Q-switched neodymium:YAG laser system (Continuum Minilite II) (24). A rapid-scanning monochromator system (RSM-1000, OLIS Instruments Inc.) was used to collect the absorption spectra from 350–750 nm (via 50 L/mm, 500-nm blaze wavelength gratings) at 1-ms resolution (24). Difference spectra were collected by using 1000 scans averaged per second. Single-wavelength kinetic measurements following light activation were also measured by averaging five traces per protein sample. Equation 1 was used for multiexponential fitting of the kinetic data,

$$y(t) = A_0[1 - e^{-(t - t_{00})/\tau_{\text{form}}}] \times \{w_1[e^{-(t - t_{00})/\tau_{d1}}] + (1 - w_1) \cdot [e^{-(t - t_{00})/\tau_{d2}}]\} \quad (\text{Eq. 1})$$

where A_0 is the absorption at the time of laser excitation, t is the time (s), t_{00} is the time of the onset of the actinic pulse (s), τ_{form} is the time constant for formation of the state, τ_{d1} and τ_{d2} are decay constants for the state, and w_1 and $(1 - w_1)$ are weight factors for τ_{d1} and τ_{d2} , respectively. All measurements were collected at 25 °C.

Author contributions—D. D. O. and D. L. T. conceived and coordinated the study. M. M. T. and E. L. D. were responsible for all aspects of the experimental program. L. B. L. and A. E. A. made significant contributions to the development of enzymatic assays and production of spectral tuning mutants. J. A. G. and R. R. B. oversaw the time-resolved spectral data acquisition and analysis. M. M. T. and D. D. O. wrote the paper. All authors discussed and commented on the manuscript.

Acknowledgments—We thank the Adar family and friends for continued support throughout this work. We appreciate the Harold S. Schwenk, Sr. Distinguished Chair in Chemistry (University of Connecticut) and support from the Brandeis University Provost's research fund. We thank Dr. Julius Rentger for invaluable help with the COPASI software. We also thank Dr. Leigh Plant for time and effort spent to guide us through the procedures for immunofluorescence staining of CHO cells.

References

- Ernst, O. P., Lodowski, D. T., Elstner, M., Hegemann, P., Brown, L. S., and Kandori, H. (2014) Microbial and animal rhodopsins: structures, functions, and molecular mechanisms. *Chem. Rev.* **114**, 126–163
- Spudich, J. L., Yang, C. S., Jung, K. H., and Spudich, E. N. (2000) Retinylidene proteins: structures and functions from archaea to humans. *Annu. Rev. Cell Dev. Biol.* **16**, 365–392
- Smith, S. O. (2010) Structure and activation of the visual pigment rhodopsin. *Annu. Rev. Biophys.* **39**, 309–328
- Palczewski, K. (2012) Chemistry and biology of vision. *J. Biol. Chem.* **287**, 1612–1619
- Avelar, G. M., Schumacher, R. I., Zaini, P. A., Leonard, G., Richards, T. A., and Gomes, S. L. (2014) A rhodopsin-guanlyl cyclase gene fusion functions in visual perception in a fungus. *Curr. Biol.* **24**, 1234–1240
- Gao, S., Nagpal, J., Schneider, M. W., Kozjak-Pavlovic, V., Nagel, G., and Gottschalk, A. (2015) Optogenetic manipulation of cGMP in cells and animals by the tightly light-regulated guanylyl-cyclase opsin CyclOp. *Nat. Commun.* **6**, 8046

7. Scheib, U., Stehfest, K., Gee, C. E., Körschen, H., Fudim, R., Oertner, T. G., and Hegemann, P. (2015) The rhodopsin-guanylyl cyclase of the aquatic fungus *Blastocladiella emersonii* enables fast optical control of cGMP signaling. *Sci. Signal.* **8**, rs8
8. Strassmaier, T. (2002) *HIV Membrane Fusion: Analysis of Novel Inhibitors*. Ph.D. thesis, Brandeis University
9. Molday, L. L., and Molday, R. S. (2014) 1D4: a versatile epitope tag for the purification and characterization of expressed membrane and soluble proteins. *Methods Mol. Biol.* **1177**, 1–15
10. Oprian, D. D., Molday, R. S., Kaufman, R. J., and Khorana, H. G. (1987) Expression of a synthetic bovine rhodopsin gene in monkey kidney cells. *Proc. Natl. Acad. Sci. U.S.A.* **84**, 8874–8878
11. Aparicio, J. G., and Applebury, M. L. (1995) The bovine photoreceptor outer segment guanylate cyclase: purification, kinetic properties, and molecular size. *Protein Expr. Purif.* **6**, 501–511
12. Marti, T., Rösselet, S. J., Otto, H., Heyn, M. P., and Khorana, H. G. (1991) The retinylidene Schiff base counterion in bacteriorhodopsin. *J. Biol. Chem.* **266**, 18674–18683
13. Mogi, T., Stern, L. J., Marti, T., Chao, B. H., and Khorana, H. G. (1988) Aspartic acid substitutions affect proton translocation by bacteriorhodopsin. *Proc. Natl. Acad. Sci. U.S.A.* **85**, 4148–4152
14. Sunahara, R. K., Beuve, A., Tesmer, J. J., Sprang, S. R., Garbers, D. L., and Gilman, A. G. (1998) Exchange of substrate and inhibitor specificities between adenylyl and guanylyl cyclases. *J. Biol. Chem.* **273**, 16332–16338
15. Tucker, C. L., Hurley, J. H., Miller, T. R., and Hurley, J. B. (1998) Two amino acid substitutions convert a guanylyl cyclase, RetGC-1, into an adenylyl cyclase. *Proc. Natl. Acad. Sci. U.S.A.* **95**, 5993–5997
16. Tesmer, J. J., Sunahara, R. K., Gilman, A. G., and Sprang, S. R. (1997) Crystal structure of the catalytic domains of adenylyl cyclase in a complex with G_αGTP γ S. *Science* **278**, 1907–1916
17. Liu, Y., Ruoho, A. E., Rao, V. D., and Hurley, J. H. (1997) Catalytic mechanism of the adenylyl and guanylyl cyclases: modeling and mutational analysis. *Proc. Natl. Acad. Sci. U.S.A.* **94**, 13414–13419
18. D'Antona, A. M., Xie, G., Sligar, S. G., and Oprian, D. D. (2014) Assembly of an activated rhodopsin-transducin complex in nanoscale lipid bilayers. *Biochemistry* **53**, 127–134
19. Xie, G., D'Antona, A. M., Edwards, P. C., Fransen, M., Standfuss, J., Schertler, G. F., and Oprian, D. D. (2011) Preparation of an activated rhodopsin/transducin complex using a constitutively active mutant of rhodopsin. *Biochemistry* **50**, 10399–10407
20. Devine, E. L., Oprian, D. D., and Theobald, D. L. (2013) Relocating the active-site lysine in rhodopsin and implications for evolution of retinylidene proteins. *Proc. Natl. Acad. Sci. U.S.A.* **110**, 13351–13355
21. Fasick, J. I., Lee, N., and Oprian, D. D. (1999) Spectral tuning in the human blue cone pigment. *Biochemistry* **38**, 11593–11596
22. Robinson, P. R., Cohen, G. B., Zhukovsky, E. A., and Oprian, D. D. (1992) Constitutively active mutants of rhodopsin. *Neuron* **9**, 719–725
23. Plant, L. D., Dementieva, I. S., Kollwe, A., Olikara, S., Marks, J. D., and Goldstein, S. A. (2010) One SUMO is sufficient to silence the dimeric potassium channel K2P1. *Proc. Natl. Acad. Sci. U.S.A.* **107**, 10743–10748
24. Ranaghan, M. J., Schwall, C. T., Alder, N. N., and Birge, R. R. (2011) Green proteorhodopsin reconstituted into nanoscale phospholipid bilayers (nanodiscs) as photoactive monomers. *J. Am. Chem. Soc.* **133**, 18318–18327
25. Omasits, U., Ahrens, C. H., Müller, S., and Wollscheid, B. (2014) Protter: interactive protein feature visualization and integration with experimental proteomic data. *Bioinformatics* **30**, 884–886
26. Hoops, S., Sahle, S., Gauges, R., Lee, C., Pahle, J., Simus, N., Singhal, M., Xu, L., Mendes, P., and Kummer, U. (2006) COPASI: a complex pathway simulator. *Bioinformatics* **22**, 3067–3074
27. Mendes, P., Messiha, H., Malys, N., and Hoops, S. (2009) Enzyme kinetics and computational modeling for systems biology. *Methods Enzymol.* **467**, 583–599

Expression, purification, and spectral tuning of RhoGC, a retinylidene/guanylyl cyclase fusion protein and optogenetics tool from the aquatic fungus *Blastocladiella emersonii*

Melissa M. Trieu, Erin L. Devine, Lindsey B. Lamarche, Aaron E. Ammerman, Jordan A. Greco, Robert R. Birge, Douglas L. Theobald and Daniel D. Oprian

J. Biol. Chem. 2017, 292:10379-10389.

doi: 10.1074/jbc.M117.789636 originally published online May 4, 2017

Access the most updated version of this article at doi: [10.1074/jbc.M117.789636](https://doi.org/10.1074/jbc.M117.789636)

Alerts:

- [When this article is cited](#)
- [When a correction for this article is posted](#)

[Click here](#) to choose from all of JBC's e-mail alerts

This article cites 26 references, 13 of which can be accessed free at <http://www.jbc.org/content/292/25/10379.full.html#ref-list-1>